# Microwave pyrolysis of olive pomace for bio-oil and bio-char production

Emily T. Kostas[1, 2§], Gabriela Durán-Jiménez[2], Benjamin J. Shepherd[2], Will Meredith[2], Lee A. Stevens[2], Orla S. A. Williams[2], Gary J. Lye[1], John P. Robinson[2]

[1]Department of Biochemical Engineering, The Advanced Centre of Biochemical Engineering, Bernard Katz Building, University College London, Gower Street, London, WC1H 6BT, UK.

[2]Faculty of Engineering, the University of Nottingham, Nottingham, NG7 2RD, U.K.

TITLE RUNNING HEAD: Microwave pyrolysis of olive pomace

§ Corresponding author

e-mail: e.kostas@ucl.ac.uk

Tel: +44 (0)20 7679 4466

**Abstract**

Olive pomace is a widely available agro-industrial waste residue in Europe that has the potential to contribute towards a circular, low carbon bio-economy. This study demonstrated, for the first time, the ability to successfully pyrolyse olive pomace with microwaves for the production of bio-char and bio-oil. It was found that the energy requirement needed to pyrolyse up to 80 % of the olive pomace was as low as 3.6 kJ/g and bio-oil yields up to 30 % were produced. Microwave power did not influence the overall yields or the chemical composition of the obtained bio-oils, but did alter the textural properties of the generated bio-chars and their ability to remove methylene blue dye. Optimum processing conditions were found to be within the 3.6 kJ/g energy requirement with a microwave power of 200 W and processing time of 180 sec. These conditions produced a bio-oil fraction containing mainly acetic acid (71.9 %) and a bio-char with a surface area of 392.3 $m^2/g$, micropore volume of 0.15 $cm^3/g$ and a methylene blue removal efficiency of 40 qMB mg/g. The results acquired from this study reveal the superiority of microwave heating in a pyrolysis system and highlight a novel and prospective route for added value recovery from natural waste resources like olive pomace.

**KEYWORDS: Microwave pyrolysis, Olive pomace, Bio-oil, Bio-char, Bioenergy**

## 1 Introduction

The new bioenergy policies that are being set by the European Union (EU) are driving to make sure that each EU Member State has their own mandatory renewable energy target to achieve by 2020; with the ultimate goal that up to at least 20 % of the EU's total energy is replaced by renewable energy sources and that all EU countries use at least 10 % biofuel in transport fuels [1, 2]. Certain EU countries are currently adopting waste bio-refinery models that utilise agricultural residues for the production of bioenergy [3] and this combination which also facilitates waste management within the EU, is assisting the transition to an efficient circular waste-based bioeconomy [4]. The EU is the world leader in the production of olive oil where around 2.1 million tonnes are produced each year, contributing to around 68 % of the world's total production [5]. Substantial amounts of OP wastes are generated in Spain, Greece and Italy as olive oil production is a major contributor to each of these countries' respective economic sectors. Currently, however, there is no EU legislation regulating the disposal of OP and current disposal practices include landfill disposal, discharge into nearby lakes, rivers or seas, and storage/evaporation in lagoons [6].

An array of studies have investigated alternative routes of processing OP in order to ensure that it is recycled back into the circular bio-economy. Studies have explored routes to convert OP into alternative forms of bioenergy, such as bioethanol [7, 8], biodiesel [9, 10] and hydrogen production (via catalytic hydrothermal gasification) [11]. Not only has it been trialled as a substrate for anaerobic digestion [12, 13], bacterial cellulose production [14] and solid-state fermentation (for xylanase and cellulase production) [15], OP has also been used as fertilizer [16, 17], tested as an adsorbent for heavy metal removal [18-20] and used as a filler based material for the development of novel polymer composites [21, 22]. Thermochemical approaches to process OP have also been studied, which include direct combustion [23-25],

gasification [26-28] and pyrolysis [29-32] to generate biofuels. Pyrolysis research has expanded in recent years due to its economical advantages and applicability within a bio-refinery to process a range of different biomass feedstocks. The process thermally decomposes biomass by heating in the absence of oxygen to temperatures between 400 and 600 °C, yielding three main products; bio-char, bio-gas and bio-oil [33]. The bio-oil fraction contains a plethora of compounds derived from cellulose, hemicellulose and lignin and can be used directly as a fuel source or blended, or as a source of platform and speciality chemicals [34]. Bio-gas has a high calorific value and can be used as biofuel to drive the process, whilst the residual bio-char can also be used either directly as a biofuel, as a soil amendment agent or activated to prepare efficient adsorbents [33].

Microwave (MW) heating has become an emerging and attractive technology to use for biomass pyrolysis compared to conventional pyrolysis, where the limitations associated with non-efficient energy transfer and slow heating rates are overcome [35, 36]. Additionally, the instantaneous volumetric heating and faster processing rates (up to ~200 sec) features associated with MW pyrolysis has the potential to produce range of specific products within the bio-oil fraction that result from the unique thermal gradients obtained in the heated biomass [35, 37, 38]. This was recently highlighted in a previous study by the authors that revealed the presence of a unique nitrogen-containing compound, L-Proline, 1-methyl-5-oxo-, methylester, in bio-oils generated from the MW pyrolysis of the seaweed *Laminaria digitata* and its extraction residue [38]. It is believed that the presence of this compound resulted from the inherently low temperatures attained in the MW pyrolysis system that was used and the fact that no MW susceptors were required in the study. Yet despite the encouraging attributes associated with MW pyrolysis, this form of green technology to process OP has never been explored in comparison to conventional pyrolysis of OP which can be found in the literature [30, 39-43].

It is imminent that alternative processing technologies are explored to establish new and compatible ways of processing OP, particularly since there are currently no regulations regarding OP disposal. Furthermore, the application of microwaves to pyrolyse biomass has significant potential within an OP biorefinery process. Therefore, the aim of this study was to gain an insight into the feasibility of conducting MW pyrolysis on OP and to identify innovative applications of generated products; rending this study the first of its kind. The utilisation of specialised MW equipment with a well-defined electric field means that the specific energies required to induce pyrolysis (without the aid of microwave susceptors) can be determined, as these parameters are imperative for potential scalability of the process. The effects of specific energy and power on mass loss, bio-oil yield and quality are addressed with attempts of optimisation being explored. In addition, the generated bio-chars were characterised and assessed as potential adsorption materials for methylene blue dye removal properties and the bio-oil were characterised to identify compound of potential industrial interest.

## 2 Materials and methods

### 2.1 Reagents

All reagents were of AnalaR grade and obtained from Sigma-Aldrich and Fisher Scientific unless otherwise specified. All water used was subjected to deionised reverse osmosis and of ≥18 mega-ohm purity.

### 2.2 Olive pomace collection and preparation for pyrolysis trials

The OP used in this study was collected from a traditional olive mill in Kalythies village, Rhodes, Greece in February 2018 and was subsequently dried in a fan oven at 80 °C for a minimum of 48 h until dry, in order to remove the majority of the water present. The OP was then milled using a disc mill (TEMA Machinery Ltd, UK) until a fine homogeneous powder was obtained. For the MW pyrolysis trials, the powdered OP was densified in an 8 ton Specac

automatic pellet press. Samples (10 g) were loaded into a 31.75 mm pellet die and loaded to 8 tons of pressure.

## 2.3 Characterisation of olive pomace

### 2.3.1 Biochemical composition

A modified version of the method described by Fukushima and Hatfield [44] was used for the quantification of lignin. OP (100 mg) was incubated with 4.0 mL of 25 % acetyl bromide (AcBr) solution (in glacial acetic acid) at 50°C for 2 h and afterward the volume was made up to 16 mL with glacial acetic. An aliquot (0.5 mL) of this solution was further diluted with glacial acetic acid (2.5 mL) and 0.3 M NaOH (1.5 mL). A 0.5 mL aliquot of 0.5 M hydroxylamine hydrochloride solution and a further 5.0 mL of glacial acetic acid were added and the absorbance at 280 nm was measured (7315 spectrophotometer; Jenway, UK). Lignin concentrations were calculated using extinction coefficient generated from corresponding measurements using lignin standards. Experiments were conducted in triplicate.

For quantification of cellulose and hemicellulose, a modified version of the Dubois assay [45] was followed where 1 mL of 12 M $H_2SO_4$ was added to 30 mg of OP and incubated at 37 °C for 1 h. Water (11 mL) was then added to the sample to dilute the acid concentration to 1 M. Samples were then incubated at 100 °C for 2 h. Liberated monosaccharides (glucose, galactose, arabinose and xylose) were analysed via Ion Chromatography using Dionex ICS-3000, using the method outlined in Kostas et al [46]. The CarboPacTM PA 20 column (3 x 150 mm) was used and the mobile phase was 10 mM NaOH with a flow rate of 0.5 mL/min. The injection volume was 10 μL and the column temperature was 30 °C. Authentic standards of monosaccharides (glucose, arabinose, galactose and xylose) with concentrations within range of 1 to 0.0625 g/L were used for monosaccharide quantification. The final monosaccharide concentrations were adjusted to an anhydrous correction factor to determine the percentage of

polysaccharides cellulose (glucose) and hemicellulose (summation of arabinose, galactose and xylose) on a dry weight basis. Experiments were conducted in triplicate.

### 2.3.2 Ultimate analysis

The elemental composition, C, H and N, of the samples was determined using a LECO CHN-628 elemental analyser using 2,5-(Bis(5-tert-butyl-2-benzo-oxazol-2-yl) thiophene (BBOT) as a standard. O was calculated by difference (100 % - (C + H + N)). Samples were analysed in triplicate.

### 2.3.3 Thermal characterisation

TGA-DSC thermal profiles were obtained using TA Instruments Q5000 TGA (New Castle, DE, USA) according to the method outlined in Lester et al [47]. In brief, samples (10-15 mg) were placed in alumina pans and heated from room temperature to 900 ºC at 5 ºC/min with a nitrogen ($N_2$) flowrate of 100 ml/min. At 900 ºC the gas was switched to air at 100 ml/min. Moisture and ash contents of the OP were determined by the produced TGA profile.

The specific heat capacity was determined by using a TA Instruments SDT Q600 TGA-DSC. The OP (10 mg) was heated from room temperature to 900ºC at 10 ºC/min with a ($N_2$) flowrate of 100 ml/min. The main output from the DSC measurement was the heat flow as a function of temperature. The heat flow values were used to calculate the temperature dependent specific heat capacity, $C_p(T)$, of the OP as shown in Eq. 1.

$$C_p(T) = \frac{-H(T)}{\frac{dT}{dt}} \quad (1)$$

where $H(T)$ is the specific heat flow to the OP (W/g) at temperature $T$ (ºC) and $dT/dt$ is the heating rate (ºC/min).

### 2.3.4 Dielectric properties

The dielectric constant (ε') and dielectric loss factor (ε") of the OP was determined using the cavity perturbation technique. The measurements were performed at 2470 MHz, from 20 to 700 °C and a detailed description of the equipment is given in Adam et al [48]. ε′ is a measure of a material's ability to store electromagnetic energy through polarisation, and ε" is a material's ability to convert this stored energy into heat [49]. ε′ and ε" can be used to assess the general ability of a material to heat in an electromagnetic field, and this quantity is known as the loss tangent, tan δ:

$$\tan \delta = \frac{\varepsilon''}{\varepsilon'} \quad (2)$$

## 2.4 Microwave pyrolysis experiments

The MW pyrolysis system used in the present study is described in Kostas et al [38] and can be seen in Fig. 1. In brief, the system was operated at frequency of 2450 ± 25 MHz and includes a generator with 2 kW maximum output power; an automatic three-stub tuner (S-TEAM STHD v1.5) connected to a rectangular WR430 waveguide. The automatic tuner was used for impedance matching, to minimise the reflected power and also to log the absorbed power over time so that an energy balance can be carried out. A cylindrical single mode $TE_{010}$ cavity was connected by WR430 waveguide to the sliding short and the incident, absorbed and reflected powers were recorded. The pyrolysis reactor consisted of a quartz tube (35 mm ID) where the pelletised sample was placed. The condenser was placed below the microwave cavity so that any bio-oils that were condensed upon contact with the cold ($N_2$) would flow under gravity to the rest of the collected bio-oil and avoid liquid droplets falling back onto the OP pellet.

Before performing any pyrolysis experiments, optimal tuner settings were determined using a vector network analyser (Rohde & Schwarz ZVL) and adjusting the stub and sliding-short positions to minimise reflected power. Since it is not possible to obtain accurate temperature measurements in MW-heating experiments [50, 51], specific absorbed energy was used instead

of temperature as a control variable. This was determined by numerical integration of the absorbed power, ($P_a$), according to the following equation:

$$E = \frac{\int P_a dt}{M} \quad (3)$$

where $E$ is the specific absorbed energy (kJ/g), $t$ is time differential (sec), and $M$ is the initial mass of the pellet (g).

Prior to running any experiments, the system was calibrated without a sample in order to ensure that no MW energy was absorbed by the MW cavity walls. Power losses were confirmed to be <5 %.

MW pyrolysis experiments on the OP were carried out at powers of 150 – 900 W for 20 – 240 sec to give specific energies of 1.8 (low), 2.4 (medium) and 3.6 (high) kJ/g, respectively (Table S1). The vapours produced during pyrolysis were quenched by a condenser and the bio-oil was collected in a flask and stored at 4 °C until further analysis (section 2.6). Any non-condensables were vented through an extraction system, as bio-gas productions and analysis was not within the scope of this study. The solid (bio-char) which remained at the end of the trials was collected, cooled and weighed to calculate the percentage mass loss. The bio-gas fraction was not collected, however the mass balanced of bio-gas was estimated by difference.

The most suitable specific energy range that produced the greatest yields of bio-oil and highest mass loss for the OP was investigated in further pyrolysis trials in order to optimise and study the influence of a narrower power range (200 – 500 W) with varying pyrolysis run times (72 – 180 sec); Table S2.

### 2.5 Prediction of temperature simulations

As it was not possible to measure the temperature that was reached during the pyrolysis experiments, the temperature distribution of 3 OP pellets (selected at random for proof of principal) that were pyrolysed within the tested specific energy groups were estimated. This was achieved using electromagnetic modelling based on the measured dielectric properties

(Section 2.3.4), the specific heat capacity (Section 2.3.3) and the thermal conductivity of OP obtained from Mason et al [52]. The Finite Element Method (FEM) was applied, using COMSOL Multiphysics 5.3 electromagnetic simulation software which involved constructing a tetrahedral mesh of the OP dimensions. Maxwell's equations were calculated to derive the magnitude of the electric field and the power density distribution (amount of power absorbed into the OP pellet). Temperature coupling of the power density as a heat source was used alongside the material properties of the OP pellet to determine the temperature reached during the MW pyrolysis process. The boundary equations required for the computational simulations are presented in Table S3.

### 2.6 Bio-oil analysis

Samples of neat (undiluted) bio-oil were analysed by gas chromatography – mass spectrometry (GC-MS) in full scan mode (m/z 40-450) on a Varian CP-3800 GC interfaced to a Varian 1200 MS (EI mode, 70 eV). Separation was achieved on a Zebron ZB-1701 fused silica capillary column (60 m x 0.25 mm i.d., 0.25 μm thickness), following injection in split mode (100:1), with Helium as the carrier gas, and an oven programme of 50°C (hold for 2 min) to 300°C (hold for 16 min) at 5 °C/min. Identification of individual compounds was performed by comparing experimental mass spectra with those in the NIST Mass Spectral library (NIST14 database; National Institute of Standards and Technology, Maryland, USA). The percentage area method was used for the quantification of the compounds present in the bio-oil, to which then the values were converted to and expressed as proportion of total identified (%).

### 2.7 Bio-char characterisation

#### 2.7.1 Ultimate and TGA analysis

Ultimate and TGA analyses were performed on the bio-chars generated from the optimisation trial by following the methodologies outlined in sections 2.3.2 and 2.3.3.

### 2.7.2 True density determination

The true density measurements of the OP and bio-chars were carried out using a Micromeritics AccuPyc II 1340 Pycnometer. Helium was used as the gas displacement medium, and all samples were dried using a vacuum oven at 120 °C for 24 hours prior to analysis. Approximately 250 mg was weighed into a 1 $cm^3$ sample cell, with the sample purged 20 times with Helium, and then 20 analysis cycles were acquired. From the 20 analysis cycles the average true density was calculated.

### 2.7.3 $CO_2$ adsorption isotherms

$CO_2$ adsorption isotherms of the OP and bio-chars were acquired using a Micromeritics ASAP 2420 instrument using $CO_2$ as the adsorbate. Prior to analysis, approximately 250 mg of samples was weighed into a sample tube and degassed to remove adsorbed moisture and other gases under high vacuum at 120 °C for 15 h. Isotherms were carried out at 0 °C from 0.00005 to 0.035 relative pressure ($P/P_0$). The surface area and micropore volume was calculated using the Dubinin-Radushkevich model using Microactive Software V5.0.

### 2.7.4 Surface morphology of OP and bio-chars

A Scanning Electron Microscope was used to image the surface morphology of the OP and any morphological changes that occurred after MW pyrolysis of the OP. The OP and bio-chars generated by MW pyrolysis at 200 and 350 W were prepared by pouring a thin layer on carbon sticky tabs that were attached to stubs. The stubs were then platinum coated (approx. 10 nm) and SEM was conducted on a FEI Quanta 600i SEM with energy dispersive X-ray. The images were scanned at ~1500x magnification and the working distance was between 12.8 – 13.2 mm.

## 2.8 Bio-char methylene blue (MB) absorption tests

Adsorption experiments were carried out using Methylene blue dye (MB) purchased from Sigma Aldrich and used without further purification. The experiments were conducted in batch

systems using 20 mg of bio-char with 10 mL of 300 mg/L MB solution in polycarbonate cylindrical cells at 30 °C using an incubator at 160 rpm. After 24 h, bio-chars were decanted from the dye solution and the remaining liquid was analysed by UV–Vis spectrophotometry employing a Hach DR-5000 spectrophotometer. Each experiment was performed in triplicate under identical conditions. The dye concentration at equilibrium was calculated from the calibration curve, which was obtained at the wavelength of maximum absorbance (664 nm). Finally, the adsorbed amount was calculated using Eq. (4)

$$q = \frac{(C_0 - C_f)}{m} \text{ x } V \quad (4)$$

where $q$ is the absorbed amount in mg/g, $C_0$ and $C_f$ are the initial and equilibrium concentrations in mg/L, $m$ is the mass of the bio-char (g), and $V$ is the volume (L).

# 3 Results and discussion

## 3.1 Biochemical, thermal and dielectric characterisation

The cellulose and hemicellulose contents were 15.9 and 13.6 % (d/w), respectively, whilst lignin represented the greatest component, contributing to 27.0 % (d/w) (Table S4). The loss tangent for the dielectric property profile is a highly non-linear function of temperature, with peaks at 100 °C, 205 °C followed by an exponential increase at temperatures in excess of 450 °C (Fig 2 A). The changes in the dielectric profile result from the chemical transformations that are occurring within the OP as temperatures increase. The dielectric property behaviour can be related to the mass loss which results from the volatilisation of the OP (Fig. 2 B). The loss tangent value of the OP at room temperature, around 0.09, is considerably higher compared to other biomass feedstocks including seaweed (*L. digitata*) [38], pecan nut shell [53] and sycamore [36] which have loss tangent values of 0.01, 0.04 and 0.055, respectively. This may be to the presence of residual oil in the OP that remains with traditional olive oil processing techniques, and usually ranges from around 18 – 27 % [54]. The high loss tangent value at

room temperature compared to other biomasses is advantageous for MW processing, as biomass feedstocks are in general poor absorbers of MW [55]. In order to overcome this barrier, MW-absorbing materials such as bio-char and silicon carbide are often mixed with the biomass to induce heating and ultimately start the pyrolysis process [56]. Yet by exploiting the OP's naturally high ability to absorb MWs, the MW pyrolysis of OP may be easily feasible without the use of MW absorbants.

### 3.2 Microwave pyrolysis trials

There was a positive trend between specific energy and mass loss, with higher energies generally leading to greater mass loss yields (Fig. 3 A). Maximum mass losses obtained in this scoping trial were between 78.0 – 80.6 % within specific energy ranges of 2.3 – 3.5 kJ/g. These specific energy requirements also take into account the energy that is required to remove any residual water from the OP pellet, during the pyrolysis process. This is the first study to report such high mass losses achieved from biomass MW pyrolysis at that particular specific energy range. Adam et al [36], who used a fluidised bed MW system to pyrolyse sycamore obtained mass loss yields between 60 – 70 % between higher specific energy range of 3.5 – 4.2 kJ/g, whilst another study that employed a different set-up of a gas-inerted fixed-bed system achieved a maximum 65 % mass loss of European Larch at a specific energy of 2.5 kJ/g [35]. In a previous study conducted by the authors using the same MW system as detailed in this work, mass loss yields of seaweed were within the ranges of 50 – 70 % at specific energies of 1.6 – 3.0 kJ/g [38]. It appears that less energy is required to pyrolyse a greater degree of the OP and this may be attributed to the relatively high dielectric properties of OP exhibited at room temperature (Fig 2 A). There also appeared to be a positive trend with bio-oil yields against energy (Fig 3 B) with the majority of bio-oil yields falling within the range of 10.0 – 28.7 %.

It is evident that there is a decrease in mass loss with an increase in MW power in the lower and medium tested energies (Fig. 3 C). On the contrary, for the higher energy range, there appeared to be no significant difference in mass loss yields as the power increased from 150 to 750 W, yet a decrease from 78.0 to 62.9 % in mass loss is seen when a power of 900 W was used. For bio-oil yields, it is clearly evident that the lowest investigated power of 150 W produced the highest yields of bio-oil across the three energy ranges, although powers investigated in the higher energy range generated greater bio-oil yields (19.4 – 38.0 %) on average (Fig. 3 D). A power of 450 W (in the higher energy range) yielded the greatest amount of bio-oil (38.0 %), however it is noticeable from Figs. 3 C and D is that the lowest power input of 150 W across the three energy ranges always generated the greatest mass loss and bio-oil yields of the pyrolysis process. This indicates that lower powers are better suited however within a higher energy range of around 3.6 kJ/g. When higher energies are applied, greater temperatures can be reached during the pyrolysis process, essentially leading to greater thermal decomposition levels (resulting in significant mass losses being attained to an extent). This is evident in the predicted OP surface temperatures depicted in Fig. 4 which match the OP bio-char images. These were simulated as accurate temperature measurements cannot be conducted within a MW system [55]. It is clear that greater temperatures were reached in the higher energy range (from 650 °C on the outside to 900 °C in the centre) compared to both the lower (100 °C on the outside to 500 °C in the centre) and medium (350 °C on the outside to 600 °C) energy ranges.

### 3.2.1 Microwave pyrolysis optimisation trial

An optimisation study was performed in order to explore the effects of lower levels of power (200 – 500 W) within the higher specific energy range (3.6 kJ/g) on mass loss and bio-oil yields. The overall mass balance of the process for each of the processing conditions can be seen in Fig S1. Interestingly, no differences in OP mass losses are evident between the powers

(and time combinations – sec) that were tested (Fig. 5). There does appear to be a slight decrease in bio-oil yields when powers exceed 350 W which may be attributed to greater temperatures being reached with the greater powers (possibly leading to gasification of the process). During gasification, there is a shift in product proportion which results in a greater bio-gas fraction and lower bio-oil yields [57]. Despite the bio-gas fraction not being collected for analysis in this study as it was beyond the scope of the work, incorporating bio-gas collection in future studies would enhance the understandings of this process with OP and would be of benefit to the overall life cycle/techno-economical assessments. However, it was not directly evident which parameters are optimal for OP processing based off the initial findings in the optimisation study. In order to gain insight, more in depth analysis was conducted on the bio-char and bio-oil fractions that were produced from OP.

### 3.3 Characterisation of bio-oil samples from OP

Bio-oils that were generated from the optimisation MW pyrolysis trial were analysed by GC-MS. Due to the high number of peaks found on the chromatograms and difficulties separating the peaks due to the complex composition of bio-oil, the most prominent compounds were semi-quantitatively evaluated and can be seen in Table 1. The bio-oils appear to have an abundance of different classes of compounds that are typically identified in bio-oils generated from lignocellulosic feedstocks; ketones, phenols, aldehydes, carboxylic acids, alcohols and anhydrosugars. Acetic acid was the main compound which was most prevalent and accounted for around 67 – 72 % of the total compounds that were identified. It is believed that the presence of acetic acid in pyrolysis bio-oil is derived from the breakdown of acetyl groups on the hemicellulose polymer [58]. Furthermore, it is known that levoglucosan is also sensitive to heat and decomposes to acetic acid at high temperatures [59], which would explain the lower levels, around 0.66 – 1.27 %, that were identified in the bio-oils generated herein. Levoglucosan is mainly a product of the β-1,4 glycosidic bond cleavage on the cellulose polymer [58] and a

prominent compound in pyrolysis bio-oil that is frequently used as a marker compound for cellulose breakdown. However, as simulated temperature profiles of the OP pellets were predicted to have reached between 650 – 900 °C in the higher tested energy range (Figs. 4 A and B), it is likely that levoglucosan underwent a secondary decomposition reaction to yield acetic acid. Various studies attempting to understand the pyrolysis mechanism of levoglucosan have also identified acetaldehyde, glycolaldehyde, 1-hydroxy-2-propanone, acetone, 3-hydroxy-2-butanone, 2,3-butanedione, furan, furfural and furfuryl alcohol as decomposition products [60, 61]. The presence of a range of phenol derivatives in the generated OP bio-oils (phenol, methoxyphenol and dimethoxyphenol) although at lower concentrations, are related to the thermal deconstruction of the principal monomers of lignin (coniferyl alcohol, p-coumaryl alcohol and synapyl alcohol) [62].

Even though it is clear that the compounds identified in the pyrolysis bio-oils are thermal degradation products of the main biochemical constituents of the OP, MW power did not directly influence bio-oil composition or favour the formation of specific compounds. However, the presence of compounds such as acetic acid, levoglucosan and phenol derivatives as raw chemical precursors, makes OP bio-oil an attractive feedstock for applications in a bio-refinery.

### 3.4 Investigating the abilities of generated OP bio-chars as methylene blue adsorbents

The elemental composition of the bio-chars are shown in Table 2 and there are clear differences in composition between the non-pyrolysed OP and the generated bio-chars. The non-pyrolysed OP is mainly composed of carbon (51.1 %), oxygen (41.0 %), hydrogen (7.14 %) and nitrogen (0.73 %), which is in agreement with the literature [63]. The percentage of carbon in the bio-chars increased from 51.1 % to be within similar ranges of 73.0 to 77.8 %. There also appeared to be an increase in ash content, as well as the density of the generated bio-chars, which is

typically expected post MW pyrolysis. However, there appeared to be no true overall effect of power on the composition of the generated OP bio-chars.

MW power does appear to influence bio-char surface area and MB adsorption abilities (Fig. 6 A). The surface areas of the generated bio-chars are significantly higher (ranging from 255.1 – 392.3 $m^2/g$) than the non-pyrolysed OP (44.7 $m^2/g$). It is evident, however, that the surface areas of the bio-chars vary non-linearly with MW power. The micropore volume of the bio-chars also displayed the exact same trend with surface area (seen in Fig 6 B), with micropore volumes ranging from 0.08 – 0.15 $cm^3/g$, yet still much higher than OP (0.02 $cm^3/g$). Interestingly, the non-pyrolysed OP removed the highest amount of MB (45.9 $q_{MB}$ mg/g), despite having the lowest surface area (Fig 6 A). This has been previously reported, nevertheless, where a MB adsorption value of 42.3 mg/g from OP was recorded, and it is known that biomass or waste residues in their natural forms are highly efficient at MB removal [64]. Traditionally, activated carbon, which has a porous structure with a large internal surface area resulting from chemical or physical activation, is the most widely used adsorbent for removing methylene blue (MB) dye from aqueous solutions. However, as commercially available activated carbons are relatively expensive, carbon adsorbents have been prepared from a number of different agricultural wastes and lignocellulosic biomasses as inexpensive and renewable alternatives via both conventional and microwave heating means [65, 66]. As such, it was important to also evaluate the abilities of the generated bio-chars to remove MB dye in this study. When waste residues such as OP are heated, the increase in the release of organic volatile compounds creates pore-like structures which enhance the surface area; simultaneously generating adequate dye adsorbing materials. This appeared to be the case for the OP bio-char that was generated by applying 200 W of power, which significantly had the highest surface area (393.3 $m^2/g$) and greatest micropore volume (0.15 $cm^3/g$) compared to the other generated bio-chars, and removed similar amounts of MB dye (41.0 $q_{MB}$ mg/g) as the non-pyrolysed OP

(45.9 $q_{MB}$ mg/g). The fact both the non-pyrolysed OP and the 200 W bio-char removed similar amounts of MB dye may be due to distinct alterations in surface chemistries. MB removal by the non-pyrolysed OP most likely results from interactions between different functional groups on the surface of the non-pyrolysed OP (such as alcoholic, carboxylic and phenolic groups) with the cationic group on the MB dye molecule [67]. Furthermore, hydrogen bonds could also be formed between the hydroxyl groups of the non-pyrolysed OP and the nitrogen atom of the MB dye [68]. On the contrary, a different mechanism of MB dye removal is predicted with the generated bio-chars. The increase in carbon and decrease in oxygen contents between the non-pyrolysed OP and the bio-chars, suggests a rearrangement of the carbon structure between the samples (from aliphatic to aromatic). This evidently enhanced the formation of porous bio-char (as seen in Figs. 6 A and B and Figs. 7 A - C). It is suggested that MB adsorption onto the generated bio-chars may be controlled by the combination of π–π and electrostatic interactions, in addition to mechanisms of intra-particle diffusion of the MB dye molecule onto the porous structures of the bio-char [69]. The SEM micrographs in Fig. 7 A - C validate these premises, as it is clear that the non-pyrolysed OP has a more organised and intact surface structure (Fig. 7 A), whereas the bio-chars generated by pyrolysing at 200 W and 350 W have a rougher texture (Fig. 7 B - C). It is also noticeable that there are more heterogeneous pores on the 200 W bio-char (Fig. 7 B) compared to the 350 W bio-char (Fig. 7 C) which was chosen for analysis due to its weaker ability to remove the MB dye; these micrographs support the results in Figs. 6 A and B. Further research to examine the OP bio-chars for the removal of a wider range of food and textile dyes as well as heavy metal ions (such as Pb (II), Cd (II), Zn (II), Ni (II), Cu (II)) would be of great interest in order to gain a better understanding of OP bio-char applications. Furthermore, the surface areas of the bio-chars generated from this optimisation study are actually higher than reported values of bio-chars produced from OP via conventional heating at 700 °C for 2 hours [70], which potentially highlights the superiority of MW heating.

## 4 Conclusions

This study has demonstrated the potential of using OP as a source of bio-oil and bio-char via MW pyrolysis. Optimum MW pyrolysis conditions were found to be within the higher specific energy range of 3.6 kJ/g for greater mass loss (ca. 80 %) and bio-oil yields (ca 26 – 30 %). The overall yield and compound composition of the bio-oil was not influenced by MW power within this specific energy range, however acetic acid was the most prominent identifiable compound in all generated bio-oils (66.5 – 71.9 %). MW power did appear to effect the textural and the MB dye adsorption properties of the bio-chars, with 200 W for 180 sec (at 3.6 kJ/g specific energy) proving to be optimal processing conditions. The findings in this work provide evidence of the exciting potential for efficient bio-refinery processes for OP to be developed.

## Acknowledgements

ETK would like to thank Mr and Mrs Sarikas (Rhodes, Greece) for providing the olive pomace. No specific grant from funding agencies in the public, commercial, or not-for-profit sectors was received at the time that this research was being conducted. However, ETK acknowledges support in the form of a Discovery Fellowship from the UK Biotechnology and Biological Sciences Research Council (BB/S010610/1) at the time this manuscript was being written and prepared for publication. GDJ acknowledges the support received from the Consejo Nacional de Ciencia y Tecnologia (CONACyT), Mexico, under the grant 389535 and OSAW thanks the University of Nottingham for support in the form of an Anne McLaren Research Fellowship.

## References


1. Union, E., *Directive 2009/28/EC of the European Parliament and of the Council of 23 April 2009 on the promotion of the use of energy from renewable sources and amending and subsequently repealing Directives 2001/77/EC and 2003/30/EC.* Official Journal of the European Union, 2009. **5**: p. 2009.
2. Zabaniotou, A., *Redesigning a bioenergy sector in EU in the transition to circular waste-based Bioeconomy-A multidisciplinary review.* Journal of Cleaner Production, 2018. **177**: p. 197-206.
3. Zabaniotou, A., et al., *Conceptual vision of bioenergy sector development in Mediterranean regions based on decentralized thermochemical systems.* Sustainable Energy Technologies and Assessments, 2017. **23**: p. 33-47.
4. Zilberman, D., et al., *Technology and the future bioeconomy.* Agricultural Economics, 2013. **44**(s1): p. 95-102.
5. Berbel, J. and A. Posadillo, *Review and analysis of alternatives for the valorisation of agro-industrial olive oil by-products.* Sustainability, 2018. **10**(1): p. 237.
6. Rodrigues, F., F.B. Pimentel, and M.B.P. Oliveira, *Olive by-products: Challenge application in cosmetic industry.* Industrial Crops and Products, 2015. **70**: p. 116-124.
7. Haagensen, F., et al., *Pre-treatment and ethanol fermentation potential of olive pulp at different dry matter concentrations.* Biomass and bioenergy, 2009. **33**(11): p. 1643-1651.
8. Fernandes, M.C., et al., *Bioethanol production from extracted olive pomace: dilute acid hydrolysis.* Bioethanol, 2016. **2**(1).
9. Che, F., et al., *Exploring a promising feedstock for biodiesel production in Mediterranean countries: a study on free fatty acid esterification of olive pomace oil.* Biomass and bioenergy, 2012. **36**: p. 427-431.
10. Rajaeifar, M.A., et al., *Environmental impact assessment of olive pomace oil biodiesel production and consumption: a comparative lifecycle assessment.* Energy, 2016. **106**: p. 87-102.
11. Sert, M., et al., *Hydrogen production from olive-pomace by catalytic hydrothermal gasification.* Journal of the Taiwan Institute of Chemical Engineers, 2018. **83**: p. 90-98.
12. Serrano, A., et al., *Performance evaluation of mesophilic semi-continuous anaerobic digestion of high-temperature thermally pre-treated olive mill solid waste.* Waste Management, 2019. **87**: p. 250-257.
13. De la Lama, D., R. Borja, and B. Rincón, *Performance evaluation and substrate removal kinetics in the semi-continuous anaerobic digestion of thermally pretreated two-phase olive pomace or "Alperujo".* Process Safety and Environmental Protection, 2017. **105**: p. 288-296.
14. Gomes, F.P., et al., *Production of bacterial cellulose by Gluconacetobacter sacchari using dry olive mill residue.* Biomass and Bioenergy, 2013. **55**: p. 205-211.
15. Leite, P., et al., *Ultrasounds pretreatment of olive pomace to improve xylanase and cellulase production by solid-state fermentation.* Bioresource technology, 2016. **214**: p. 737-746.
16. Montemurro, F., G. Convertini, and D. Ferri, *Mill wastewater and olive pomace compost as amendments for rye-grass.* Agronomie, 2004. **24**(8): p. 481-486.
17. Arvanitoyannis, I.S. and A. Kassaveti, *Current and potential uses of composted olive oil waste.* International journal of food science & technology, 2007. **42**(3): p. 281-295.
18. Petrov, N., et al., *Conversion of olive wastes to volatiles and carbon adsorbents.* Biomass and Bioenergy, 2008. **32**(12): p. 1303-1310.
19. Fiol, N., et al., *Sorption of Pb (II), Ni (II), Cu (II) and Cd (II) from aqueous solution by olive stone waste.* Separation and Purification technology, 2006. **50**(1): p. 132-140.
20. Pagnanelli, F., et al., *Heavy metal removal by olive pomace: biosorbent characterisation and equilibrium modelling.* Chemical Engineering Science, 2003. **58**(20): p. 4709-4717.

21. Lammi, S., et al., *Dry fractionation of olive pomace as a sustainable process to produce fillers for biocomposites.* Powder Technology, 2018. **326**: p. 44-53.
22. Kaya, N., et al., *Fabrication and characterization of olive pomace filled PP composites.* Composites Part B: Engineering, 2018. **150**: p. 277-283.
23. Guizani, C., et al., *Combustion characteristics and kinetics of torrefied olive pomace.* Energy, 2016. **107**: p. 453-463.
24. Buratti, C., et al., *Thermal behaviour and kinetic study of the olive oil production chain residues and their mixtures during co-combustion.* Bioresource technology, 2016. **214**: p. 266-275.
25. Williams, O., et al., *Overcoming the caking phenomenon in olive mill wastes.* Industrial crops and products, 2017. **101**: p. 92-102.
26. Vera, D., et al., *Experimental and economic study of a gasification plant fuelled with olive industry wastes.* Energy for Sustainable Development, 2014. **23**: p. 247-257.
27. Liliedahl, T., et al., *Defluidisation of fluidised beds during gasification of biomass.* Biomass and bioenergy, 2011. **35**: p. S63-S70.
28. La Cal Herrera, J., F. Jurado, and B. Ogayar, *A new model of energy valorization for olive grove by-products based on the gasification technology integrated in an olive-oil mill.* International journal of green energy, 2012. **9**(7): p. 661-672.
29. Ghouma, I., et al., *Pyrolysis of olive pomace: degradation kinetics, gaseous analysis and char characterization.* Waste and biomass valorization, 2017. **8**(5): p. 1689-1697.
30. Martín-Lara, M., et al., *The role of temperature on slow pyrolysis of olive cake for the production of solid fuels and adsorbents.* Process Safety and Environmental Protection, 2019. **121**: p. 209-220.
31. Guida, M., et al., *Thermochemical treatment of olive mill solid waste and olive mill wastewater.* Journal of Thermal Analysis and Calorimetry, 2016. **123**(2): p. 1657-1666.
32. Lajili, M., et al., *Fast pyrolysis and steam gasification of pellets prepared from olive oil mill residues.* Energy, 2018. **150**: p. 61-68.
33. Bridgwater, A., D. Meier, and D. Radlein, *An overview of fast pyrolysis of biomass.* Organic geochemistry, 1999. **30**(12): p. 1479-1493.
34. Vispute, T.P., et al., *Renewable chemical commodity feedstocks from integrated catalytic processing of pyrolysis oils.* Science, 2010. **330**(6008): p. 1222-1227.
35. Robinson, J., et al., *Microwave pyrolysis of biomass: control of process parameters for high pyrolysis oil yields and enhanced oil quality.* Energy & Fuels, 2015. **29**(3): p. 1701-1709.
36. Adam, M., et al., *Microwave fluidized bed for biomass pyrolysis. Part II: Effect of process parameters.* Biofuels, Bioproducts and Biorefining, 2017. **11**(4): p. 613-624.
37. Shepherd, B., et al., *Microwave pyrolysis of biomass within a liquid medium.* Journal of analytical and applied pyrolysis, 2018. **134**: p. 381-388.
38. Kostas, E.T., et al., *Microwave pyrolysis of Laminaria digitata to produce unique seaweed-derived bio-oils.* Biomass and Bioenergy, 2019. **125**: p. 41-49.
39. Şensöz, S., İ. Demiral, and H.F. Gerçel, *Olive bagasse (Olea europea L.) pyrolysis.* Bioresource technology, 2006. **97**(3): p. 429-436.
40. Zabaniotou, A., et al., *Olive residues (cuttings and kernels) rapid pyrolysis product yields and kinetics.* Biomass and bioenergy, 2000. **18**(5): p. 411-420.
41. Pütün, A.E., et al., *Bio-oil from olive oil industry wastes: Pyrolysis of olive residue under different conditions.* Fuel Processing Technology, 2005. **87**(1): p. 25-32.
42. Uzun, B.B., A.E. Pütün, and E. Pütün, *Composition of products obtained via fast pyrolysis of olive-oil residue: effect of pyrolysis temperature.* Journal of Analytical and Applied Pyrolysis, 2007. **79**(1-2): p. 147-153.
43. Demirbas, A., *Producing bio-oil from olive cake by fast pyrolysis.* Energy Sources, Part A: Recovery, Utilization, and Environmental Effects, 2007. **30**(1): p. 38-44.

44. Fukushima, R.S. and R.D. Hatfield, *Comparison of the acetyl bromide spectrophotometric method with other analytical lignin methods for determining lignin concentration in forage samples.* Journal of agricultural and food chemistry, 2004. **52**(12): p. 3713-3720.
45. Dubois, M., et al., *Colorimetric method for determination of sugars and related substances.* Analytical chemistry, 1956. **28**(3): p. 350-356.
46. Kostas, E.T., et al., *Selection of yeast strains for bioethanol production from UK seaweeds.* Journal of applied phycology, 2016. **28**(2): p. 1427-1441.
47. Lester, E., M. Gong, and A. Thompson, *A method for source apportionment in biomass/coal blends using thermogravimetric analysis.* Journal of analytical and applied pyrolysis, 2007. **80**(1): p. 111-117.
48. Adam, M., et al., *Microwave fluidized bed for biomass pyrolysis. Part I: Process design.* Biofuels, Bioproducts and Biorefining, 2017. **11**(4): p. 601-612.
49. Robinson, J., et al., *Understanding microwave heating effects in single mode type cavities-theory and experiment.* Physical Chemistry Chemical Physics, 2010. **12**(18): p. 4750-4758.
50. Pert, E., et al., *Temperature measurements during microwave processing: the significance of thermocouple effects.* Journal of the American Ceramic Society, 2001. **84**(9): p. 1981-1986.
51. Mazubert, A., et al., *Key role of temperature monitoring in interpretation of microwave effect on transesterification and esterification reactions for biodiesel production.* Bioresour Technol, 2014. **161**: p. 270-9.
52. Mason, P., et al., *Comparative study of the thermal conductivity of solid biomass fuels.* Energy & Fuels, 2016. **30**(3): p. 2158-2163.
53. Jimenez, G.D., et al., *New insights into microwave pyrolysis of biomass: Preparation of carbon-based products from pecan nutshells and their application in wastewater treatment.* Journal of Analytical and Applied Pyrolysis, 2017. **124**: p. 113-121.
54. Galanakis, C.M., *Olive fruit dietary fiber: components, recovery and applications.* Trends in Food Science & Technology, 2011. **22**(4): p. 175-184.
55. Kostas, E.T., D. Beneroso, and J.P. Robinson, *The application of microwave heating in bioenergy: A review on the microwave pre-treatment and upgrading technologies for biomass.* Renewable and Sustainable Energy Reviews, 2017. **77**: p. 12-27.
56. Beneroso, D., et al., *Microwave pyrolysis of biomass for bio-oil production: Scalable processing concepts.* Chemical Engineering Journal, 2017. **316**: p. 481-498.
57. Bridgwater, A.V., *Review of fast pyrolysis of biomass and product upgrading.* Biomass and bioenergy, 2012. **38**: p. 68-94.
58. Wu, Y.-m., et al., *Low temperature pyrolysis characteristics of major components of biomass.* Journal of Fuel Chemistry and Technology, 2009. **37**(4): p. 427-432.
59. Demirbaş, A., *Mechanisms of liquefaction and pyrolysis reactions of biomass.* Energy conversion and management, 2000. **41**(6): p. 633-646.
60. Guo, S., et al., *Quantitative study of the pyrolysis of levoglucosan to generate small molecular gases.* RSC Advances, 2019. **9**(33): p. 18791-18802.
61. Li, S., et al., *Real-time evolved gas analysis by FTIR method: an experimental study of cellulose pyrolysis.* Fuel, 2001. **80**(12): p. 1809-1817.
62. Mohan, D., C.U. Pittman Jr, and P.H. Steele, *Pyrolysis of wood/biomass for bio-oil: a critical review.* Energy & fuels, 2006. **20**(3): p. 848-889.
63. Windeatt, J.H., et al., *Characteristics of biochars from crop residues: potential for carbon sequestration and soil amendment.* Journal of environmental management, 2014. **146**: p. 189-197.
64. Banat, F., et al., *Bench-scale and packed bed sorption of methylene blue using treated olive pomace and charcoal.* Bioresource technology, 2007. **98**(16): p. 3017-3025.
65. Duran-Jimenez, G., et al., *Adsorption of dyes with different molecular properties on activated carbons prepared from lignocellulosic wastes by Taguchi method.* Microporous and Mesoporous Materials, 2014. **199**: p. 99-107.

66. Durán-Jiménez, G., et al., *Pb (II) removal using carbon adsorbents prepared by hybrid heating system: Understanding the microwave heating by dielectric characterization and numerical simulation.* Journal of Molecular Liquids, 2019. **277**: p. 663-671.
67. Rizzi, V., et al., *An interesting environmental friendly cleanup: The excellent potential of olive pomace for disperse blue adsorption/desorption from wastewater.* Dyes and Pigments, 2017. **140**: p. 480-490.
68. Doğan, M., H. Abak, and M. Alkan, *Adsorption of methylene blue onto hazelnut shell: kinetics, mechanism and activation parameters.* Journal of Hazardous Materials, 2009. **164**(1): p. 172-181.
69. Durán-Jiménez, G., et al., *Fast regeneration of activated carbons saturated with textile dyes: Textural, thermal and dielectric characterization.* Chemical Engineering Journal, 2019.
70. Pellera, F.-M. and E. Gidarakos, *Effect of dried olive pomace–derived biochar on the mobility of cadmium and nickel in soil.* Journal of Environmental Chemical Engineering, 2015. **3**(2): p. 1163-1176.

**TABLE CAPTIONS**

**Table 1. Composition of bio-oils obtained from the optimised microwave pyrolysis trial.**

**Table 2. Characterisation of OP bio-chars obtained after optimised microwave pyrolysis trial.**

**FIGURE CAPTIONS**

**Fig 1. Schematic of microwave pyrolysis rig used in this study.**

**Fig 2. A) Dielectric properties (Loss Tangent), B) TGA (solid line)/DSC (dotted line) and C) specific heat capacity of olive pomace as a function of temperature.**

**Fig 3. A) Mass loss and B) bio-oil yields of OP against specific energy and the influence of power on C) mass loss and D) bio-oil yield within each energy group.**

**Fig 4. A) OP pellets post pyrolysis within energy ranges of 1.8, 2.4 and 3.6 kJ/g and simulated and B) temperature distribution**

**Fig 5. Influence of power on mass loss and bio-oil yields during microwave pyrolysis optimisation study.**

**Fig 6. Effect of power on the generated bio-char surface area and their methylene blue removal abilities, compared to non-pyrolysed OP.**

**Fig 7. SEM images of the OP (A), bio-char generated from 200 W (B) and bio-char generated from 350 W (C) at ~1500x magnification.**

Table 1

| Compound Name | Retention Time (min) | Proportion of Total Identified (%) | | | | | | |
|---|---|---|---|---|---|---|---|---|
| | | Run 1* | Run 2* | Run 3* | Run 4* | Run 5* | Run 6* | Run 7* |
| Acetone | 5.072 | 0.34 | 0.63 | 0.31 | 0.97 | 1.45 | 0.14 | 0.62 |
| Acetic acid methyl ester | 5.131 | 0.63 | 0.77 | 0.52 | 0.64 | 0.77 | 0.37 | 0.56 |
| Acetic acid ethenyl ester | 5.922 | 0.34 | 0.34 | 0.34 | 0.39 | 0.40 | 0.46 | 0.24 |
| Acetic acid | 7.250 | 71.96 | 70.51 | 70.46 | 70.91 | 66.52 | 71.00 | 71.87 |
| Hydroxypropanone | 8.125 | 12.45 | 12.74 | 13.31 | 13.07 | 15.06 | 12.10 | 13.35 |
| Propanoic acid | 9.597 | 1.04 | 1.07 | 0.95 | 1.08 | 1.13 | 0.84 | 0.95 |
| Hydroxybutanone | 10.556 | 3.87 | 4.06 | 3.99 | 4.20 | 4.72 | 4.15 | 3.87 |
| Furfural | 12.316 | 0.24 | 0.33 | 0.20 | 0.41 | 0.33 | 0.48 | 0.35 |
| Cyclopentenone | 12.351 | 0.71 | 0.68 | 0.71 | 0.55 | 0.73 | 0.56 | 0.55 |
| Furanmethanol | 13.565 | 0.42 | 0.40 | 0.40 | 0.32 | 0.28 | 0.49 | 0.19 |
| Butanediol | 13.755 | 1.07 | 1.10 | 1.01 | 1.06 | 1.20 | 1.08 | 1.04 |
| Cyclohexanone | 15.691 | 0.41 | 0.42 | 0.33 | 0.23 | 0.22 | 0.51 | 0.18 |
| Hydroxybutanoic acid | 17.071 | 0.76 | 0.78 | 0.77 | 0.71 | 0.77 | 0.75 | 0.66 |
| Furanone | 17.331 | 0.51 | 0.54 | 0.59 | 0.58 | 0.64 | 0.65 | 0.53 |
| Methylcyclopentanedione | 18.694 | 1.40 | 1.56 | 1.56 | 1.27 | 1.49 | 1.61 | 1.25 |
| Phenol | 19.531 | 0.25 | 0.34 | 0.35 | 0.35 | 0.36 | 0.28 | 0.35 |
| Methoxyphenol | 20.121 | 1.10 | 1.29 | 1.10 | 0.93 | 1.04 | 1.16 | 0.94 |
| Methylcyclopentanediol | 21.300 | 0.71 | 0.65 | 0.80 | 0.66 | 0.76 | 0.85 | 0.65 |
| Dimethoxyphenol | 28.207 | 1.13 | 1.19 | 1.32 | 0.91 | 1.06 | 1.26 | 0.87 |
| Levoglucosan | 35.963 | 0.66 | 0.61 | 0.98 | 0.79 | 1.05 | 1.27 | 0.99 |

Table 2

| Sample | Power (W) | Time (sec) | C % | H % | N % | *O % | $Ash (%) | $Moisture (%) | True Density (g/cm$^3$) |
|---|---|---|---|---|---|---|---|---|---|
| Olive | - | - | 51.1 ± 0.4 | 7.1 ± 0.1 | 0.7 ± 0.1 | 41.0 ± 0.4 | 1.6 ± 0.3 | 6.9 ± 0.6 | 1.3 ± 0.01 |
| 1* | 200 | 180 | 77.7 ± 0.3 | 1.7 ± 0.1 | 1.3 ± 0.1 | 19.4 ± 0.4 | 9.8 ± 0.7 | 4.7 ± 0.2 | 1.7 ± 0.01 |
| 2* | 250 | 144 | 77.8 ± 0.7 | 1.7 ± 0.3 | 1.3 ± 0.1 | 19.3 ± 1.0 | 10.8 ± 0.2 | 5.4 ± 0.6 | 1.6 ± 0.01 |
| 3* | 300 | 120 | 73.5 ± 1.0 | 3.2 ± 0.5 | 1.0 ± 0.1 | 22.3 ± 1.5 | 8.6 ± 0.4 | 5.0 ± 0.3 | 1.7 ± 0.01 |
| 4* | 350 | 103 | 76.7 ± 0.9 | 2.0 ± 0.1 | 1.2 ± 0.1 | 20.1 ± 1.0 | 10.2 ± 0.3 | 4.3 ± 0.2 | 1.6 ± 0.01 |
| 5* | 400 | 90 | 77.3 ± 0.2 | 2.9 ± 0.1 | 1.3 ± 0.1 | 18.5 ± 0.2 | 7.4± 0.3 | 4.5 ± 0.1 | 1.6 ± 0.01 |
| 6* | 450 | 80 | 76.9 ± 1.0 | 2.5 ± 0.2 | 1.3 ± 0.1 | 19.4 ± 1.1 | 8.4 ± 0.2 | 4.7 ± 0.1 | 1.3 ± 0.01 |
| 7* | 500 | 72 | 75.5 ± 1.4 | 2.4 ± 0.3 | 1.9 ± 0.1 | 20.9 ± 1.6 | 9.6 ± 0.1 | 5.1 ± 0.1 | 1.6 ± 0.01 |

* Calculated by difference

$ Determined from TGA

Fig. 1

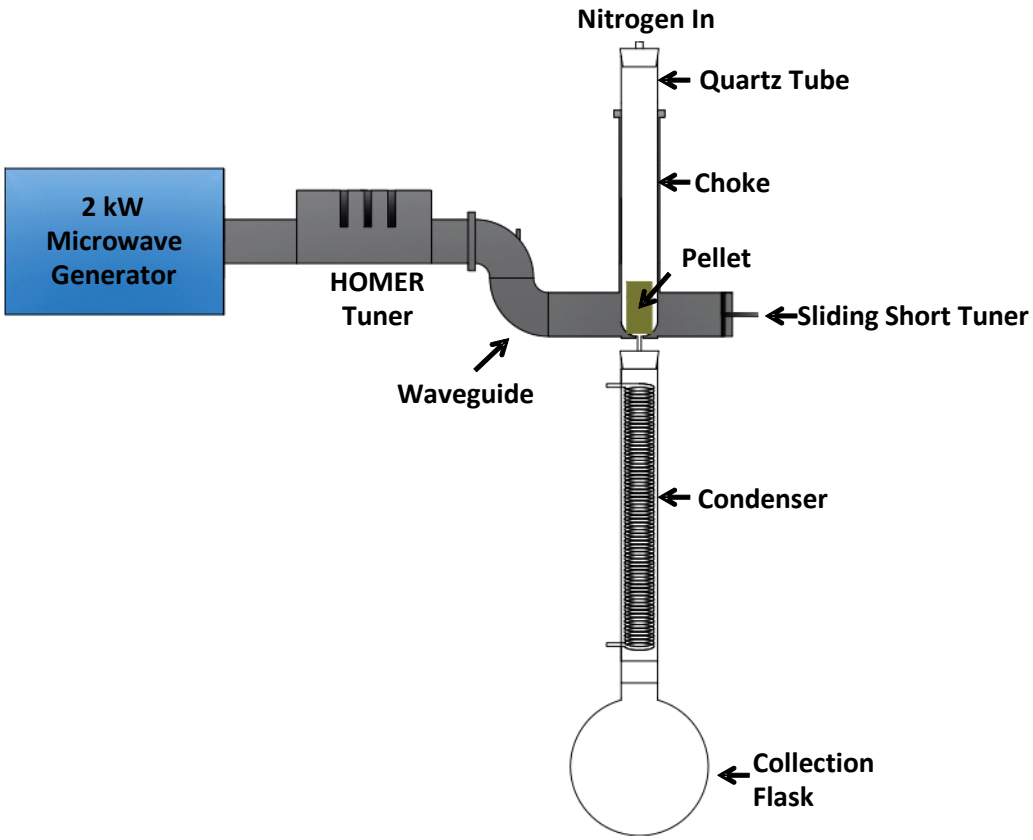
Nitrogen In
Quartz Tube
Choke
2 kW
Microwave
Generator
HOMER
Tuner
Pellet
Sliding Short Tuner
Waveguide
Condenser
Collection
Flask

Fig. 2

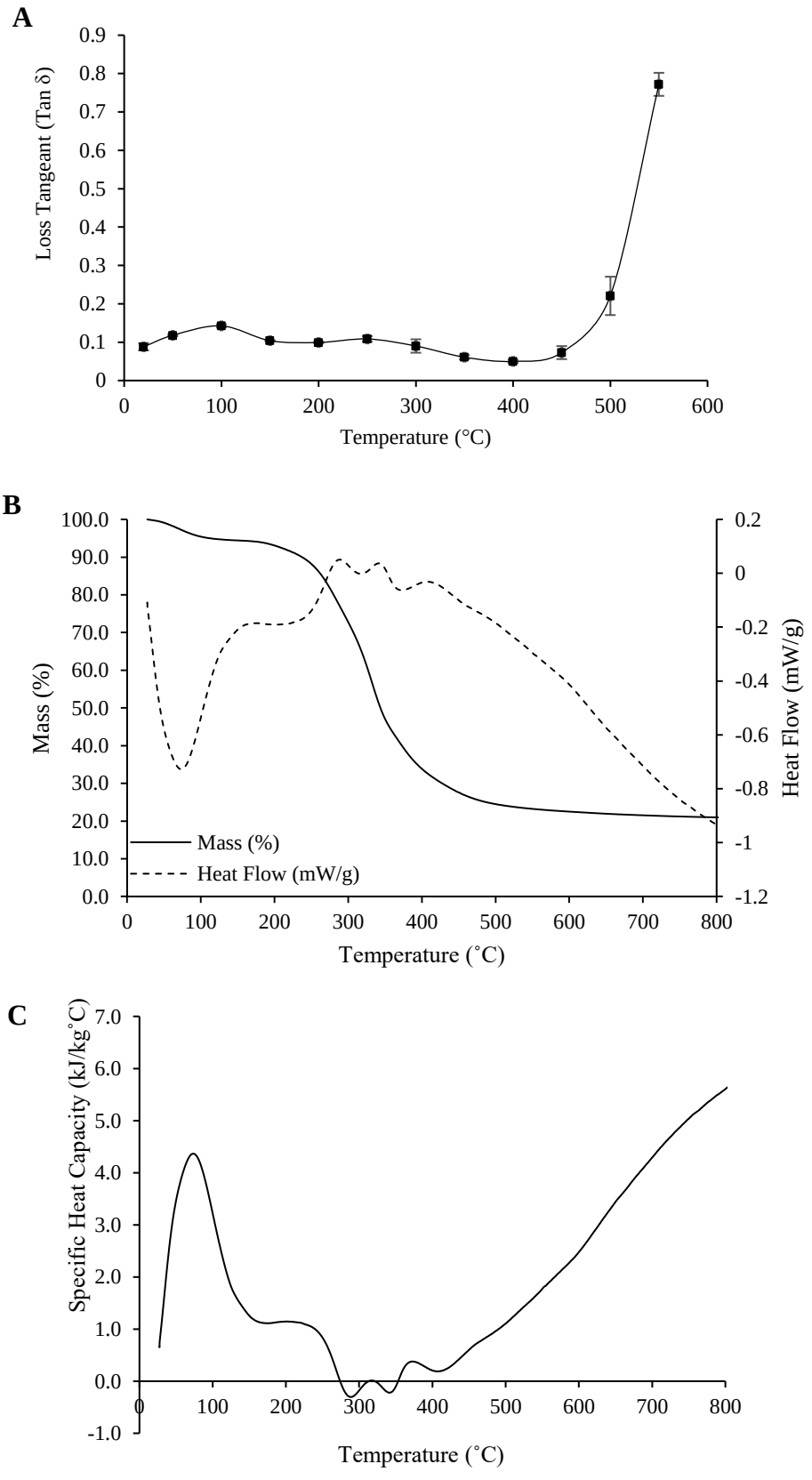
A
Loss Tangeant (Tan δ)
0.9
0.8
0.7
0.6
0.5
0.4
0.3
0.2
0.1
0
0
100
200
300
400
500
600
Temperature (°C)
B
Mass (%)
Heat Flow (mW/g)
100.0
90.0
80.0
70.0
60.0
50.0
40.0
30.0
20.0
10.0
0.0
0.2
0
-0.2
-0.4
-0.6
-0.8
-1
-1.2
0
100
200
300
400
500
600
700
800
Temperature (˚C)
C
Specific Heat Capacity (kJ/kg˚C)
7.0
6.0
5.0
4.0
3.0
2.0
1.0
0.0
-1.0
0
100
200
300
400
500
600
700
800
Temperature (˚C)

Fig. 3

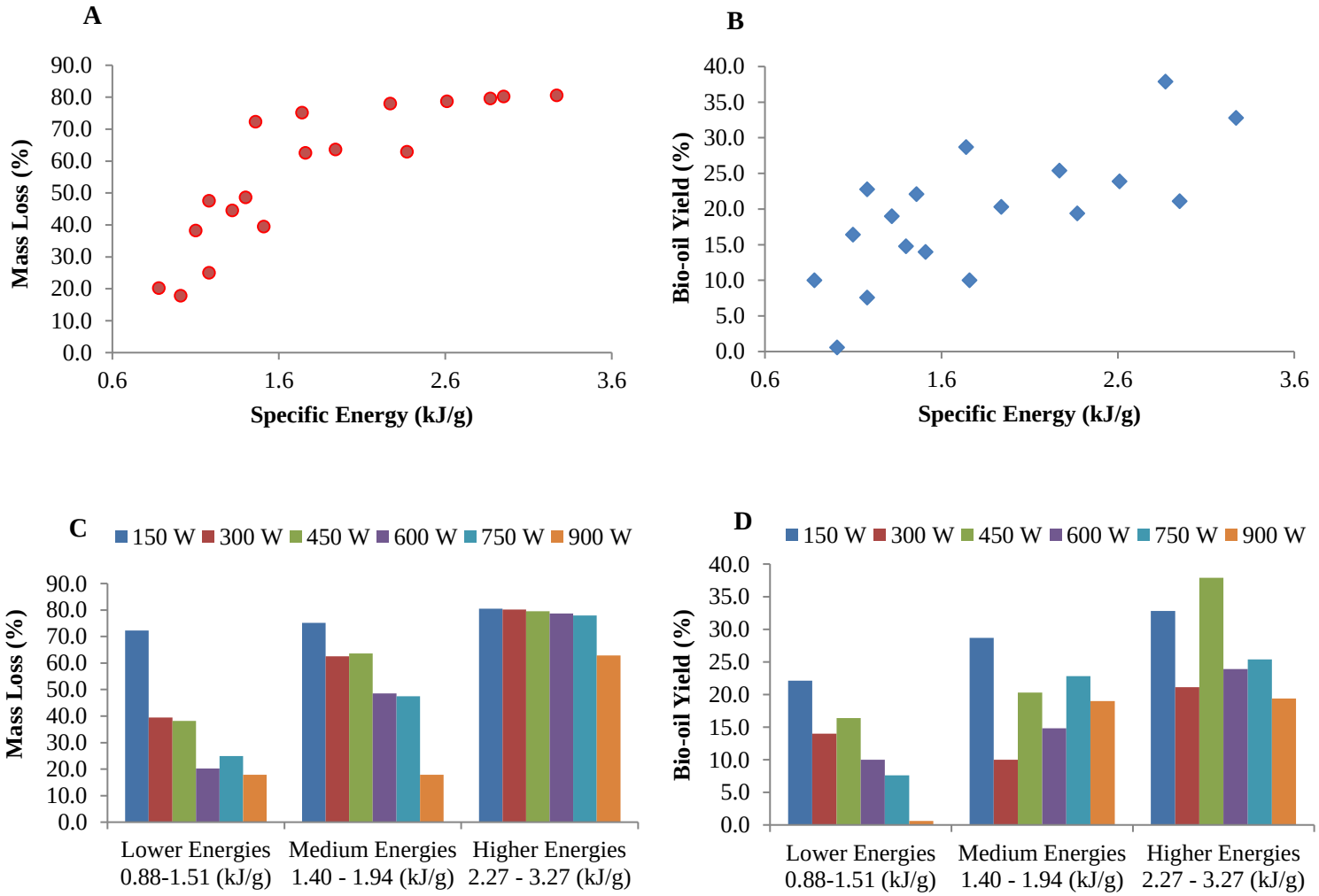
A
Mass Loss (%)
90.0
80.0
70.0
60.0
50.0
40.0
30.0
20.0
10.0
0.0
0.6
1.6
2.6
3.6
Specific Energy (kJ/g)
B
Bio-oil Yield (%)
40.0
35.0
30.0
25.0
20.0
15.0
10.0
5.0
0.0
0.6
1.6
2.6
3.6
Specific Energy (kJ/g)
C
150 W
300 W
450 W
600 W
750 W
900 W
Mass Loss (%)
90.0
80.0
70.0
60.0
50.0
40.0
30.0
20.0
10.0
0.0
Lower Energies 0.88-1.51 (kJ/g)
Medium Energies 1.40 - 1.94 (kJ/g)
Higher Energies 2.27 - 3.27 (kJ/g)
D
150 W
300 W
450 W
600 W
750 W
900 W
Bio-oil Yield (%)
40.0
35.0
30.0
25.0
20.0
15.0
10.0
5.0
0.0
Lower Energies 0.88-1.51 (kJ/g)
Medium Energies 1.40 - 1.94 (kJ/g)
Higher Energies 2.27 - 3.27 (kJ/g)

Fig. 4

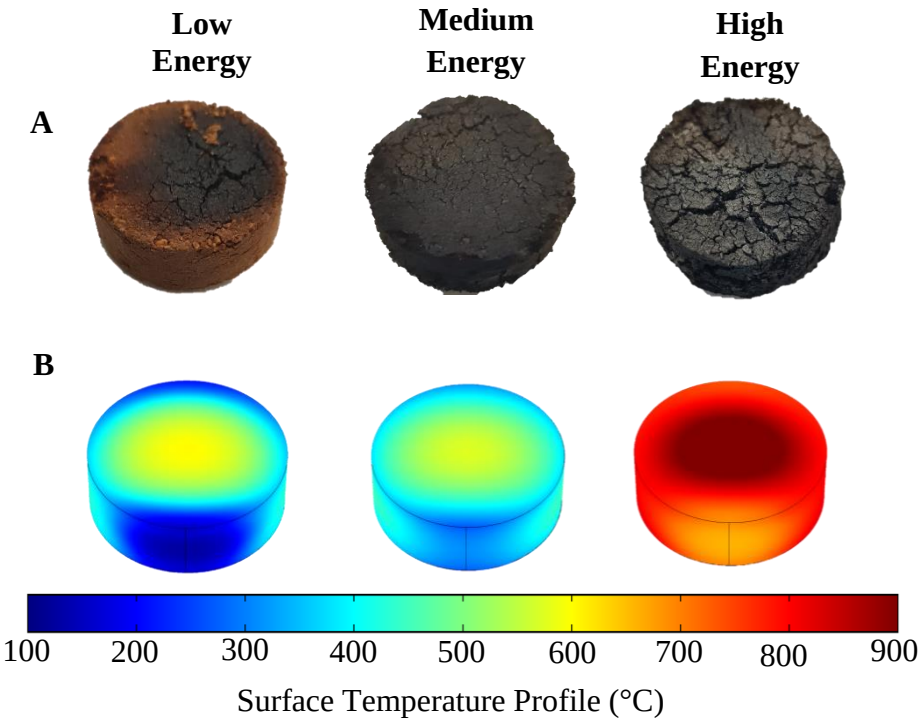
Low Energy
Medium Energy
High Energy
A
B
100
200
300
400
500
600
700
800
900
Surface Temperature Profile (°C)

Fig. 5

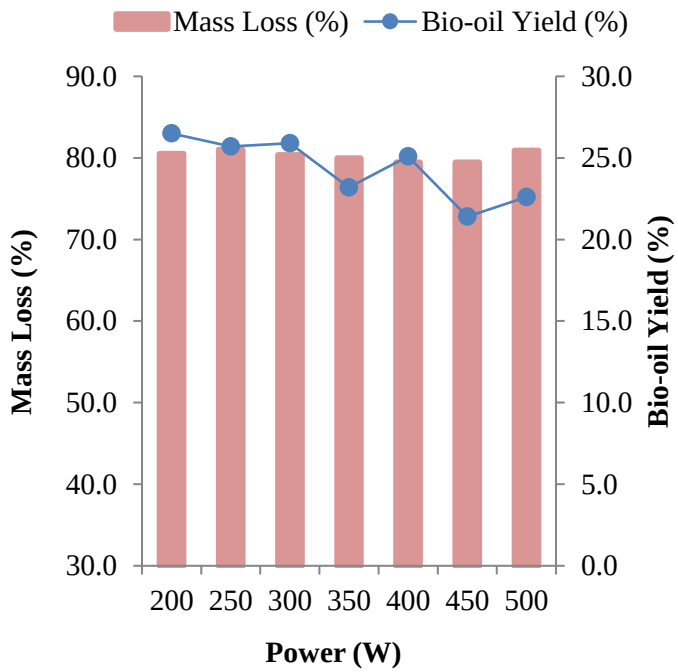
Mass Loss (%)
Bio-oil Yield (%)
90.0
80.0
70.0
60.0
50.0
40.0
30.0
30.0
25.0
20.0
15.0
10.0
5.0
0.0
Mass Loss (%)
Bio-oil Yield (%)
200 250 300 350 400 450 500
Power (W)

Fig. 6

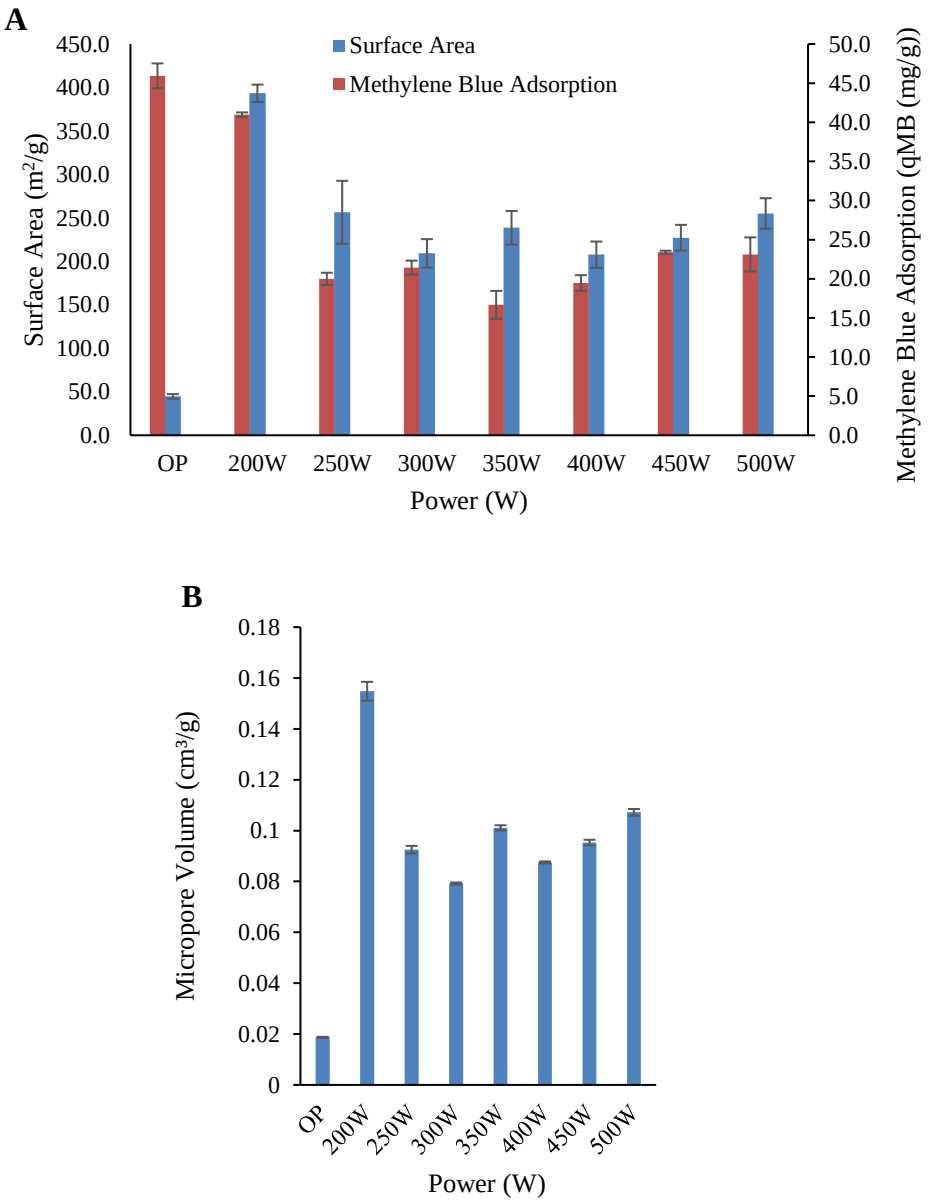
A
Surface Area
Methylene Blue Adsorption
Surface Area (m²/g)
Methylene Blue Adsorption (qMB (mg/g))
450.0
400.0
350.0
300.0
250.0
200.0
150.0
100.0
50.0
0.0
50.0
45.0
40.0
35.0
30.0
25.0
20.0
15.0
10.0
5.0
0.0
OP
200W
250W
300W
350W
400W
450W
500W
Power (W)
B
Micropore Volume (cm³/g)
0.18
0.16
0.14
0.12
0.1
0.08
0.06
0.04
0.02
0
OP
200W
250W
300W
350W
400W
450W
500W
Power (W)

Fig. 7

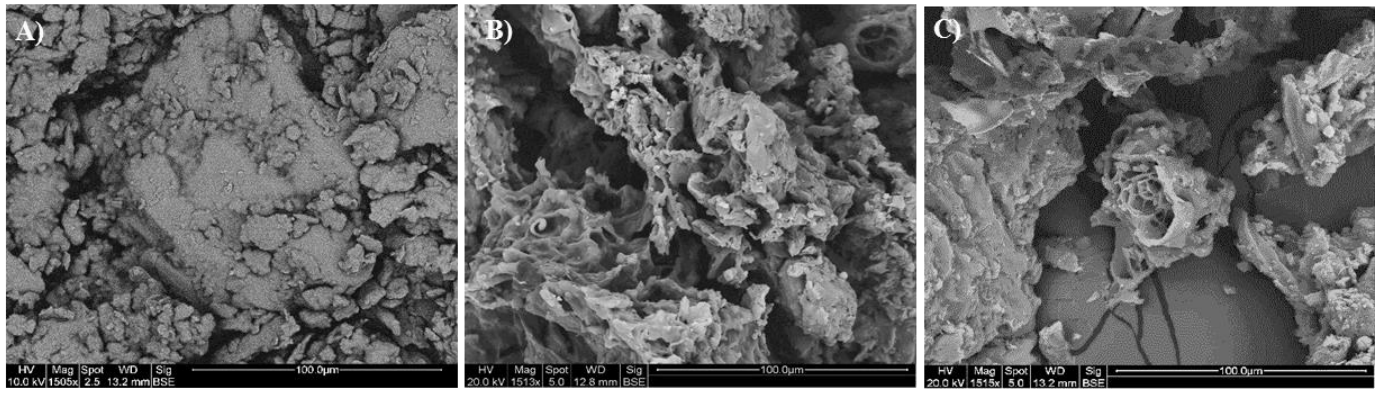
A)
HV Mag Spot WD Sig
10.0 kV 1505x 2.5 13.2 mm BSE
100.0µm
B)
HV Mag Spot WD Sig
20.0 kV 1513x 5.0 12.8 mm BSE
100.0µm
C)
HV Mag Spot WD Sig
20.0 kV 1515x 5.0 13.2 mm BSE
100.0µm